

Chemical abundances in the secondary star of the X-ray binary Cygnus X-2

L. Suárez-Andrés^{1,2}, J.I. González Hernández^{1,2}, G. Israelian^{1,2}, J. Casares^{1,2} and R. Rebolo^{1,2,3}

¹ Instituto de Astrofísica de Canarias, E-38205 La Laguna, Tenerife, Spain

² Depto. Astrofísica, Universidad de La Laguna (ULL), E-38206 La Laguna, Tenerife, Spain

³ Consejo Superior de Investigaciones Científicas, Spain

Abstract

Spectroscopic data of low-mass X-ray binaries (LMXB) can provide valuable information on supernova properties. In these systems the companion star is probably close enough to be polluted by some of the matter ejected during the supernova (SN) event of the progenitor of the compact object. We present high-resolution spectra, acquired with UES@WHT, of the LMXB Cygnus X-2. We derive the stellar parameters of the companion, taking into account any possible veiling from the accretion disk surrounding the NS. We have studied the chemical abundances, including α -elements and some Fe-peak elements to search for signatures of chemical anomalies that could have been imprinted on the secondary star in the SN event. We find a super-solar Fe content in the companion star, and an abundance enhancement in most of the studied elements. Our results suggest that the secondary star may have captured a significant amount of the ejected matter during the SN explosion. We explore different explosion models to explain these abundance anomalies.

1 Introduction

Cygnus X-2 is one of the few LMXB in which the spectrum of the nondegenerate star is visible, contributing about 50% of the total flux; with a neutron star of $M_{\text{NS}} = 1.71 \pm 0.21 M_{\odot}$ [3, 5]. It is also one of the brightest and most massive systems known to date.

The chemical composition of secondary stars in black hole and neutron star X-ray binaries have been studied for several systems, such as Nova Scorpii 1994 [14, 11] or Centaurus X-4 [10, 4]. In these studies, the authors have taken into account different scenarios of pollution from a SN event that presumably originated the compact object in these systems.

We use high resolution spectra to derive the stellar parameters and chemical abundances of the secondary star in the neutron star X-ray binary (NSXB) Cygnus X-2 with the aim of obtaining information about its formation and evolution.

2 Observations

2.1 Secondary spectrum

We obtained ten 1800-3600s spectra with the Utrecht Echelle Spectrograph (UES) attached to the 4.2-m William Herschel Telescope (WHT) at the Observatorio del Roque de Los Muchachos on 1999 July 25-26, covering the spectral regions $\lambda\lambda 5300 - 9000\text{\AA}$ at a resolving power $\lambda/\Delta\lambda \approx 36,000$. For more information about the observations see [5].

3 Chemical Analysis

3.1 Stellar parameters

The chemical analysis of secondary stars in LMXB systems is influenced by three important factors: veiling from the accretion disk, rotational broadening and S/N. We selected 6 absorption features containing relatively strong Fe lines with different excitation potentials. In order to compute synthetic spectra for these features, we adopted the atomic line data from VALD and used a grid of LTE models of atmospheres provided by R. L. Kurucz. For further details see [12]

We generated a grid of synthetic spectra for these features in terms of five free parameters, three regarding the star atmospheric model (effective temperature, T_{eff} , surface gravity, $\log g$, and metallicity, $[\text{Fe}/\text{H}]$) and two more parameters to take into account any possible veiling. These parameters were modified in steps of 100K for T_{eff} , 0.1 for $\log g$, $[\text{Fe}/\text{H}]$ and veiling, and 0.00004 for m_o . A rotational broadening of 34.6 km s^{-1} and a limb darkening of $\epsilon = 0.5$ were assumed based on [5]. A fixed microturbulence of $\xi = 2 \text{ km s}^{-1}$ was adopted.

The observed spectrum was compared with the 750,000 synthetic spectra in the grid via a χ^2 minimization procedure that provided the best model fit. Using a bootstrap Monte Carlo method, we define the 1σ confidence regions for the five parameters. Confidence regions were determined using 1000 realizations. The histograms for the results showed a big uncertainty regarding the value of $\log g$, that affects the rest of our values. We decided then not to set this parameter as a free parameter, leaving only four free and calculating them for each $\log g$ in the same range. We chose the $\log g$ that provided us with the lowest sigma, according to the gaussian fit of the distribution of MonteCarlo events of each parameter, for the four parameters, $\log g = 2.8$. The most likely values are: $T_{\text{eff}} = 6900 \pm 200\text{K}$, $\log g = 2.80 \pm 0.20$, $[\text{Fe}/\text{H}] = 0.35 \pm 0.10$, $f_{4500} = 1.55 \pm 0.15$, and $m_o = -0.00027 \pm 0.00004$.

3.2 Stellar abundances

Using the derived stellar parameters, we analyzed several spectral regions for elements such as Al, Si, S, O, among others. Each of these spectral regions were compared with two templates: WASP-17 and HR6189, properly broadened with the same rotational broadening as the secondary star in our system. We determined the abundances of those elements by comparing the observed spectrum with a grid of synthetic spectra through a χ^2 minimization

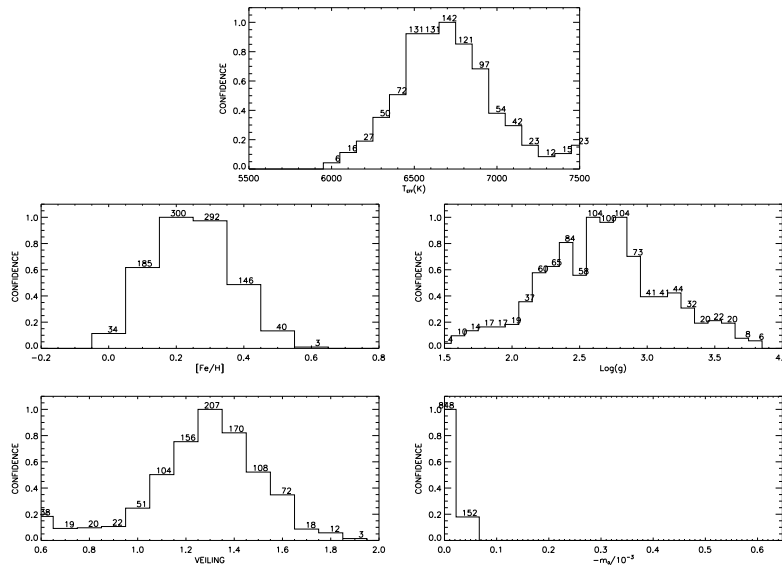


Figure 1: Distribution obtained for each parameter using Monte Carlo simulations with four free parameters. The bottom-right panel shows the distribution obtained for the veiling slope m_o , given as $-m_o/10^{-3}$ in units of \AA . The labels at the top of each bin indicate the number of simulations consistent with the bin value. The total number of simulations was 1000.

procedure. We modified the element abundances, while the stellar parameters and the veiling value were fixed [see e.g. for further details [12]]. A preliminary estimation of Fe abundance was obtained in the procedure described above and improve taking into account 9 additional Fe lines: we obtained Fe abundance of $[\text{Fe}/\text{H}] = 0.27 \pm 0.19$, where the error takes into account the dispersion of the abundances inferred from these features and the continuum noise.

Abundances for some of the studied the elements are listed in Table 1 and are referred to the solar values adopted from [13], except oxygen, taken from [9]. We stress that the major source for the errors is the inaccuracy in the location of the continuum caused by the S/N and the rotational broadening of the lines.

4 Discussion

The metallicity obtained for this object is higher than solar, and similar to the metallicity obtained in another NSXB such as Cen X-4 (see [10]). Although the sample may not be statistically significant, the metallicities of BHXBs seems to be lower. The detection of high Fe abundances in secondary stars of NSXBs may be an indication of an explosive event.

We search for anomalies in the abundance pattern of the secondary star by comparing our results with Galactic trends (see Fig. 2), adopted from [1]. For oxygen, we used the latest results from [2]. Results for sulphur were taken from [8]. As it is shown in Fig. 2, most of

Table 1: Chemical abundances and uncertainties. The oxygen abundance has been corrected for NLTE effects, $\Delta_{\text{NLTE}} = -0.3$, based on the NLTE corrections in [19]. n gives the number of lines studied for that element. Li abundance is expressed as: $\log \epsilon(\text{Li})_{\text{NLTE}} = \log[N(\text{Li})/N(\text{H})]_{\text{NLTE}} + 12$.

| Elem. | [X/H] | n | Elem. | [X/H] | n | Elem. | [X/H] | n |
|-------|-----------------|----|-------|-----------------|---|-------|------------------|---|
| Fe | 0.27 ± 0.19 | 15 | Ca | 0.27 ± 0.33 | 4 | O | -0.20 ± 0.35 | 1 |
| Mg | 0.87 ± 0.24 | 1 | Sc | 0.42 ± 0.30 | 1 | Ti | 0.59 ± 0.31 | 2 |
| Al | 0.42 ± 0.24 | 2 | Ni | 0.52 ± 0.27 | 1 | Si | 0.52 ± 0.22 | 3 |
| Li | < 1.48 | 1 | S | 0.52 ± 0.24 | 3 | | | |

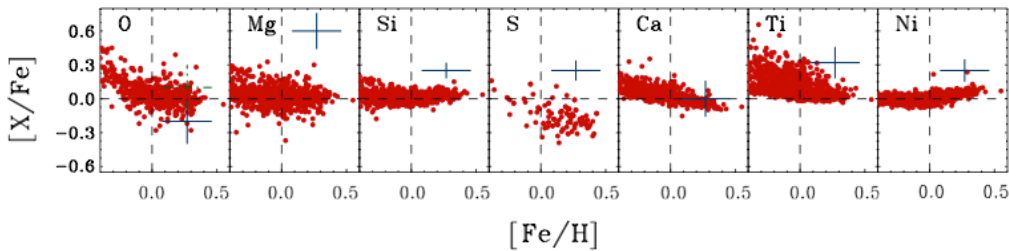


Figure 2: Element abundance ratios $[X/\text{Fe}]$ of the secondary star. Crosses indicate our obtained abundance values with errors, while full dots are the abundances of galactic field stars from [1], except for oxygen and sulphur, taken from [2] and [8], respectively. For oxygen we display two values: LTE (dotted-dashed cross) and the other one in NLTE (solid cross)

the elements in Cygnus X-2 show overabundances when compared with Galactic trends, with the exception calcium (also Al and Sc, not displayed).

4.1 Spherical SN explosion

It has been proposed that LMXBs begin their lives as wide binaries and evolve through a common-envelope phase in which the companion spirals into the massive star's envelope (see e.g. [21, 7, 17]). The helium core of the massive star evolves and ends its life as a supernova, leaving behind a neutron star or a black hole remnant. Part of the ejected mass in the SN explosion may have been captured by the secondary star, as has been found in other LMXBs such as Nova Sco 94 [14, 11]. We also consider this scenario for Cygnus X-2.

Cygnus X-2 is quite a particular X-ray binary. The stellar parameters obtained suggest that the secondary is a F2IV star. The primary star is a the neutron star of $M_{\text{NS},f} = 1.71 \pm 0.20 M_{\odot}$ and the mass ratio of the system is $q_f = 0.34 \pm 0.02$ [5], yielding a secondary mass $M_{2,f} = 0.60 \pm 0.13 M_{\odot}$. A main sequence star of this mass would have an effective temperature of 4000 K which is in conflict with the observed F-type spectrum [6, 20].

The secondary star in Cygnus X-2 might have lost a significant amount of its initial mass through mass-transfer [15, 18]. Podsiadlowski & Rappaport [18] propose an evolutionary

scenario where the secondary star has an initial mass of $M_{2,i} = 3.5M_{\odot}$, and suffers a large mass loss near the end of the main sequence. Thus we adopt different scenarios for the SN model, as the initial mass of the secondary is unknown. The input parameters of our models are basically $M_{2,i} = [2.0 - 3.5]M_{\odot}$, the initial mass of the NS is $M_{\text{NS},i} \sim 1.4M_{\odot}$ and the radius of the secondary star is obtained using pre-main sequence stellar evolutionary tracks from [20]. (See [10] and references therein).

Assuming a pre-SN circular orbit and an instantaneous spherically symmetric ejection, one can estimate the pre-SN orbital separation, a_0 (see [22]). Some of the matter ejected in the SN explosion is expected to be captured by the secondary star, polluting its atmosphere with SN nucleosynthetic products. The fraction of the matter ejected in the direction of the secondary star that is captured is controlled by the parameter f_{cap} [for further details, [12]].

We consider spherically symmetric supernova models for a $\sim 16M_{\odot}$ progenitor star with a $M_{\text{He}} \sim 4.0M_{\odot}$ He core [16], and an initial pre-explosion mass for the secondary star of $M_{2,i} = 2.0M_{\odot}$. Different values for the initial mass of the secondary star at e.g. about $M_{2,i} = 3.5M_{\odot}$ would provide similar results for lower $a_{c,i}$ and higher f_{cap} values. One could then obtain different values for the expected abundances by modifying $a_{c,i}$ and f_{cap} in each case. We assume that the secondary star had solar abundances before pollution. Our model computations take into account three different mass cut values, m_{cut} , which are typically very similar to initial and final mass of the neutron star. Dependence of the mass cut is only important for elements with Z greater than 20. (see Fig 3) In order to fit the low oxygen abundance a relatively low capture efficiency, $f_{\text{cap}} \leq 30\%$ is required, whereas more of the elements are reasonably reproduced for higher f_{cap} values.

4.2 Aspherical SN explosion

The spherically symmetric supernova explosion is not the only plausible scenario for this system. An aspherical explosion produces nucleosynthetic inhomogeneities dependent on direction: thus, if the jet in the aspherical explosion is collimated perpendicular to the orbital plane, where the secondary star is located, elements such as Ti, Ni and Fe are ejected in the jet direction, while elements like O, Mg, Al, Si and S are ejected in the equatorial plane of the helium star [16] and thus expected to be enhanced in the secondary star.

Following the procedure in the spherical case, we have considered two different asphericals models (depending of the direction of the jet). In these cases, dependence on the mass cut is important for elements heavier than Al. Contrary to the case of the spherical case, the Mg abundance can be approximately reproduced by the aspherical explosion, although Al and Sc are marginally reproduced in that case (See Fig.3).

The unusual nature of the secondary star, as studied by [15, 18], already makes it difficult to assess the evolutionary status of the system. This comparison using both spherically and aspherically symmetric SN models allow us to evaluate different scenarios but we cannot rule out any model. Taking into account the limitations in both the quality of the data and SN models available, and our simple model of contamination of the secondary star, we suggest an aspherical SN explosion of a $4M_{\odot}$ He core as the origin of the neutron star in Cygnus X-2. This result seems to be the opposite as proposed in [10], where a spherically symmetric SN

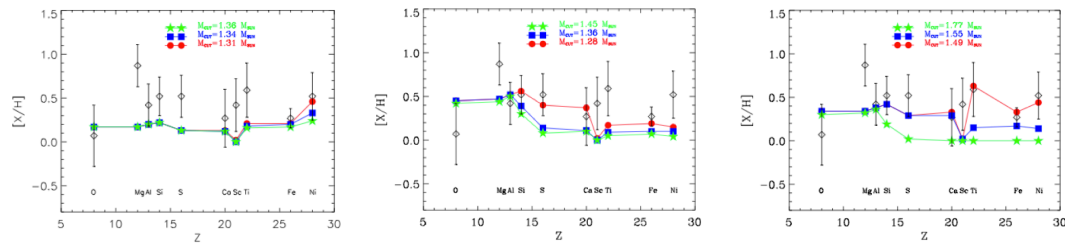


Figure 3: On the left panel, expected abundances in the secondary star’s atmosphere due to the pollution caused by a spherically symmetric core-collapsed SN explosion model. In the middle and right panel, expected abundances caused by a non-spherical explosion.

explosion provided better agreement with the observed abundances.

References

- [1] Adibekyan, V. Z., Sousa, S. G., Santos, N. C., et al. 2012, *A&A*, 545, A32
- [2] Bertrán de Lis, S. et al., 2014, in preparation
- [3] Casares, J., Charles, P., & Kuulkers, E. 1998, *ApJL*, 493, L39
- [4] Casares, J., Bonifacio, P., González Hernández, J. I., Molaro, P., & Zoccali, M. 2007, *A&A*, 470, 1033
- [5] Casares, J., González Hernández, J. I., Israelian, G., & Rebolo, R. 2010, *MNRAS*, 401, 2517
- [6] D’Antona, F., & Mazzitelli, I. 1994, *ApJs*, 90, 467
- [7] de Kool, M., van den Heuvel, E. P. J., & Pylyser, E. 1987, *A&A*, 183, 47
- [8] Ecuivillon, A., Israelian, G., Santos, N. C., et al. 2004, *A&A*, 426, 619
- [9] Ecuivillon, A., Israelian, G., Santos, N. C. et al. 2006, *A&A*, 445, 633
- [10] González Hernández, J. I., Rebolo, R., Israelian, G., et al. 2005, *ApJ*, 630, 495
- [11] González Hernández, J. I., Rebolo, R., & Israelian, G. 2008, *A&A*, 478, 203
- [12] González Hernández, J. I., Casares, J., Rebolo, R., et al. 2011, *ApJ*, 738, 95
- [13] Grevesse, N., Noels, A., & Sauval, A. J. 1996, *Cosmic Abundances*, 99, 117
- [14] Israelian, G., Rebolo, R., Basri, G., Casares, J., & Martín, E. L. 1999, *Nature*, 401, 142
- [15] King, A. R., & Ritter, H. 1999, *MNRAS*, 309, 253
- [16] Maeda, K., Nakamura, T., Nomoto, K., et al. 2002, *ApJ*, 565, 405
- [17] Nelemans, G., & van den Heuvel, E. P. J. 2001, *A&A*, 376, 950
- [18] Podsiadlowski, P., & Rappaport, S. 2000, *ApJ*, 529, 946
- [19] Przybilla, N., Butler, K., Becker, S. R., Kudritzki, R. P., & Venn, K. A. 2000, *A&A*, 359, 1085
- [20] Siess, L., Dufour, E., & Forestini, M. 2000, *A&A*, 358, 593
- [21] van den Heuvel, E. P. J. 1983, *Accretion-Driven Stellar X-ray Sources*, 303
- [22] van den Heuvel, E. P. J., & Habets, G. M. H. J. 1984, *Nature*, 309, 598